

Finite-temperature Mott transitions in multi-orbital Hubbard model

Kensuke Inaba, Akihisa Koga, Sei-ichiro Suga, and Norio Kawakami
Department of Applied Physics, Osaka University, Suita, Osaka 565-0871, Japan
 (Dated: July 1, 2020)

We investigate the Mott transitions in the multi-orbital Hubbard model at half-filling by means of the self-energy functional approach. The phase diagrams are obtained at finite temperatures for the Hubbard model with up to four-fold degenerate bands. We discuss how the first-order Mott transition points U_{c1} and U_{c2} as well as the critical temperature T_c depend on the orbital degeneracy. It is elucidated that enhanced orbital fluctuations play a key role to control the Mott transitions in the multi-orbital Hubbard model.

PACS numbers: 71.30.+h, 71.10.Fd

I. INTRODUCTION

The Mott transition has been one of the most attractive topics in strongly correlated electron systems.^{1,2} There are a number of prototype materials in transition metal oxides. A well-known example is V_2O_3 ,^{3,4} which exhibits the first-order metal-insulator transition at a certain critical temperature. The phase diagram obtained by systematic experiments is consistent with theoretical studies of the single orbital Hubbard model by means of dynamical mean field theory (DMFT).^{5,6} This implies that the DMFT treatment of the Hubbard model, which properly takes into account local electron correlations, captures the essence of the Mott transition. However, in order to give more quantitative discussions about the Mott transitions, it is indispensable to incorporate the effect of the orbital degeneracy, which often gives rise to rich phase diagrams, as observed for $La_{1-x}Sr_xMnO_3$,⁷ $RTiO_3$ ^{8,9}, etc. More recently, the orbital-selective Mott transition has attracted considerable attention,^{10,11,12,13,14,15,16} in connection with the materials such as $Ca_{2-x}Sr_xRuO_4$ ¹⁷ and $La_{n+1}Ni_nO_{3n+1}$ ^{18,19}.

These interesting experimental findings have stimulated a number of theoretical works on the Mott transitions in the two-orbital Hubbard model by means of DMFT.^{12,13,14,15,16,20,21,22,23,24,25,26,27,28,29,30,31,32} Although the two-orbital model has been studied in detail, a systematic study on the systems having more orbitals is still lacking at finite temperatures. For example, the finite-temperature Mott transitions for the multi-orbital Hubbard models has not been investigated quantitatively by DMFT. One of the difficulties lies in the practical calculation within the DMFT framework. Quantum Monte Carlo simulations, which can be a powerful numerical method to treat local correlations in DMFT, encounter sign problems. Also, Wilson's renormalization group method gets more difficult to apply as the number of orbitals increases. A much more simplified approach, the two-site DMFT,³³ is not efficient enough to treat finite-temperature properties. It is thus desirable to systematically investigate electron correlations in the multi-orbital Hubbard model at finite temperatures.

Motivated by the above hot topics, we consider the

Mott transitions in the multi-orbital Hubbard model at zero as well as finite temperatures. For this purpose, we make use of a self-energy functional approach (SFA) proposed by Potthoff recently.^{34,35} This method, which is based on the Luttinger-Ward functional approach,³⁶ gives a powerful tool to discuss electron correlations. A remarkable point is that this approach provides an efficient way to deal with finite-temperature properties of the multi-orbital Hubbard model. The main purpose of the present paper is to determine the finite-temperature phase diagram of the Hubbard model with up to four-fold bands, and quantitatively discuss how the orbital degeneracy affects the Mott transitions.

The paper is organized as follows. In the next section, we introduce the model Hamiltonian and briefly summarize the formulation of SFA. In Sec. III we present the detailed analysis based on SFA by exploiting the two-orbital model as a prototype system. Then in Sec. IV we determine the phase diagram, and discuss the nature of the Mott transitions in multi-orbital systems in detail. A brief summary is given in Sec. V.

II. MODEL AND METHOD

We consider a correlated electron system having M degenerate orbitals, which is described by the following multi-orbital Hubbard Hamiltonian,

$$\mathcal{H} = \mathcal{H}_0 + \mathcal{H}', \quad (1)$$

$$\mathcal{H}_0 = \sum_{\langle i,j \rangle} \sum_{\alpha=1}^M \sum_{\sigma} t_{\alpha} c_{i\alpha\sigma}^{\dagger} c_{j\alpha\sigma}, \quad (2)$$

$$\begin{aligned} \mathcal{H}' = & U \sum_i \sum_{\alpha=1}^M n_{i\alpha\uparrow} n_{i\alpha\downarrow} \\ & + U' \sum_i \sum_{\alpha < \alpha'=1}^M \sum_{\sigma\sigma'} n_{i\alpha\sigma} n_{i\alpha'\sigma'}, \end{aligned} \quad (3)$$

where $c_{i\alpha\sigma}^{\dagger}$ ($c_{i\alpha\sigma}$) creates (annihilates) an electron with spin σ ($=\uparrow, \downarrow$) and orbital α ($= 1, 2, 3 \dots, M$) at the i th lattice site, t_{α} denotes the hopping integral for orbital α , U (U') is the intra-orbital (inter-orbital) Coulomb interaction. In the following, we mainly consider the case of

$U = U'$, and give brief discussions for more general cases including the Hund coupling in the end of the paper.

In order to address the Mott transitions in the multi-orbital Hubbard model, we use SFA.^{34,35} We briefly summarize the essence of SFA. For a correlated electron system, the grand potential is generally expressed as

$$\Omega[\Sigma] = F[\Sigma] + \text{Tr} \ln [-(\mathbf{G}_0^{-1} - \Sigma)^{-1}], \quad (4)$$

where $F[\Sigma]$ is the Legendre transformation of the Luttinger-Ward potential $\Phi[\mathbf{G}]$, and \mathbf{G} (\mathbf{G}_0) and Σ are the full (bare) Green's function and the self-energy, respectively. The condition imposed on the functional (4),

$$\frac{\partial \Omega[\Sigma]}{\partial \Sigma} = 0, \quad (5)$$

gives the Dyson equation $\mathbf{G}^{-1} = \mathbf{G}_0^{-1} - \Sigma$. An important point is that the functional form of $F[\Sigma]$ does not depend on the detail of the Hamiltonian \mathcal{H}_0 as far as the interaction term $\mathcal{H}'(\mathbf{U})$ keeps its shape unchanged. This fact allows us to introduce a proper reference system having the same interaction term, which we denote as $\mathcal{H}_{\text{ref}} = \mathcal{H}_0(\mathbf{t}') + \mathcal{H}'(\mathbf{U})$. Then the grand potential is written as,

$$\begin{aligned} \Omega[\Sigma(\mathbf{t}')] &= \Omega(\mathbf{t}') \\ &+ \text{Tr} \ln [-(\mathbf{G}_0(\mathbf{t}')^{-1} - \Sigma(\mathbf{t}'))^{-1}] \\ &- \text{Tr} \ln [-(\mathbf{G}_0(\mathbf{t}')^{-1} - \Sigma(\mathbf{t}'))^{-1}], \end{aligned} \quad (6)$$

where $\Omega(\mathbf{t}')$ and $\Sigma(\mathbf{t}')$ are the grand potential and the self-energy for the reference system, whose bare Green's function is denoted as $\mathbf{G}_0(\mathbf{t}')^{-1} = \omega + \mu - \mathbf{t}'$ (μ : chemical potential). The variational condition (5) is rewritten as

$$\frac{\partial \Omega[\Sigma(\mathbf{t}')] }{\partial \mathbf{t}'} = 0. \quad (7)$$

By choosing the parameters \mathbf{t}' for the reference system so as to satisfy the condition (7), we can find the best system within the reference Hamiltonian, which can approximately describe the original correlated system.

It should be noticed here that SFA provides us with an efficient and tractable way to deal with finite-temperature properties of the multi-orbital system, where standard DMFT combined with numerical techniques faces difficulties in a practical computation when the number of orbitals increases. Another notable point in this approach is that the critical behavior can be discussed more precisely than the DMFT analysis,⁵ when one chooses the same type of the effective impurity model. In fact, by comparing the results obtained by the two-site DMFT,^{33,37} the critical point for a single orbital Hubbard model obtained by SFA with the two-site model³⁴ is in good agreement with that obtained by DMFT with the aid of numerical techniques.^{38,39,40}

To discuss the multi-orbital Hubbard model (3), we exploit the Anderson impurity model as a reference system

in SFA.^{34,35} The Hamiltonian for the reference system is explicitly given as

$$\mathcal{H}_{\text{ref}} = \sum_i \mathcal{H}_{\text{ref}}^{(i)}, \quad (8)$$

$$\begin{aligned} \mathcal{H}_{\text{ref}}^{(i)} &= \sum_{\alpha\sigma} \varepsilon_{0\alpha}^{(i)} c_{i\alpha\sigma}^\dagger c_{i\alpha\sigma} + \sum_{k=1}^{N_b} \sum_{\alpha\sigma} \varepsilon_{k\alpha}^{(i)} a_{k\alpha\sigma}^{(i)\dagger} a_{k\alpha\sigma}^{(i)} \\ &+ \sum_{k=1}^{N_b} \sum_{\alpha\sigma} V_{k\alpha}^{(i)} (c_{i\alpha\sigma}^\dagger a_{k\alpha\sigma}^{(i)} + H.c.) \\ &+ U \sum_{\alpha} n_{i\alpha\uparrow} n_{i\alpha\downarrow} + U' \sum_{\alpha < \alpha'} \sum_{\sigma\sigma'} n_{i\alpha\sigma} n_{i\alpha'\sigma'}, \end{aligned} \quad (9)$$

where $a_{k\alpha\sigma}^{(i)\dagger}$ ($a_{k\alpha\sigma}^{(i)}$) creates (annihilates) an electron with σ spin and α orbital at the k ($= 1, 2, \dots, N_b$) th site, which is connected to the i th site in the original lattice. Since we consider the Mott transitions without symmetry breaking, we set $\varepsilon_{k\alpha}$ and $V_{k\alpha}$ site-independent. Note that in the limit of $N_b \rightarrow \infty$, Eq. (7) is equivalent to the self-consistent equation in DMFT.³⁴ Since the Green's function and the self-energy are diagonal with respect to the site, spin, and orbital indices, the grand potential per site reads

$$\begin{aligned} \Omega/L &= \Omega_{\text{imp}} \\ &- 2 \sum_{\alpha} \int d\omega f(\omega) R_{\alpha} [\omega + \mu - \Sigma_{\alpha}(\omega)] \\ &+ 2 \sum_{\alpha} \sum_{k=0}^{N_b} \int d\omega f(\omega) \theta[G'_{k\alpha}(\omega)], \end{aligned} \quad (10)$$

$$G'_{0\alpha}(\omega) = [\omega + \mu - \varepsilon_{0\alpha} - \Delta_{\alpha}(\omega) - \Sigma_{\alpha}(\omega)]^{-1}, \quad (11)$$

$$G'_{k\alpha}(\omega) = (\omega + \mu - \varepsilon_{k\alpha})^{-1}, \quad (k = 1, 2, \dots, N_b), \quad (12)$$

$$\Delta_{\alpha}(\omega) = \sum_{k=1}^{N_b} V_{k\alpha}^2 G'_{k\alpha}(\omega), \quad (13)$$

where $R_{\alpha}(\omega) = \int_{-\infty}^{\omega} \rho_{\alpha}(z) dz$, $f(\omega) = 1/(1 + e^{-\beta\omega})$ and $\theta(\omega)$ is a step function. The grand potential and the self-energy for an impurity system $\mathcal{H}_{\text{ref}}^{(i)}$ are denoted as Ω_{imp} and $\Sigma_{\alpha}(\omega)$.

In the following, we focus on the half-filled Hubbard model ($\mu = (M - 1/2)U$) to discuss how the orbital degeneracy ($M = 1, 2, 3, 4$) affects the Mott transitions. We take the simplest reference system ($N_b = 1$), where we fix the parameters $(\varepsilon_{0\alpha}, \varepsilon_{1\alpha}, V_{1\alpha}) = (0, \mu, V)$ for each orbital α . This simplified treatment is somewhat analogous to the two-site DMFT at zero temperature. However, the present approach enables us to treat finite-temperature quantities systematically, which is a notable advantage beyond the two-site DMFT. The condition (7) is now reduced to $\partial\Omega/\partial V = 0$. We note that the hopping integral V between a given site on the original lattice and a fictitious site corresponds, roughly speaking, to the renormalized bandwidth of quasi-particles. In fact, Fermi-liquid properties at zero temperature are determined by

the value of V . For instance, small V implies the formation of heavy quasi-particles, and the system enters the insulating phase at $V = 0$. By calculating the effective hybridization V , we thus discuss the stability of the metallic state in the multi-orbital systems.

III. DETAIL OF CALCULATIONS: TWO-ORBITAL SYSTEM

Let us start with the two-orbital Hubbard model, by which we illustrate the basic procedure of SFA to determine the phase diagram for more general multi-orbital cases. We adopt here a semielliptic density of states $\rho(\varepsilon) = (\pi/W)\sqrt{1 - (2\varepsilon/W)^2}$ with the bandwidth $W = 4$.

We first look at the ground-state properties by examining the stationary points in the grand potential. In

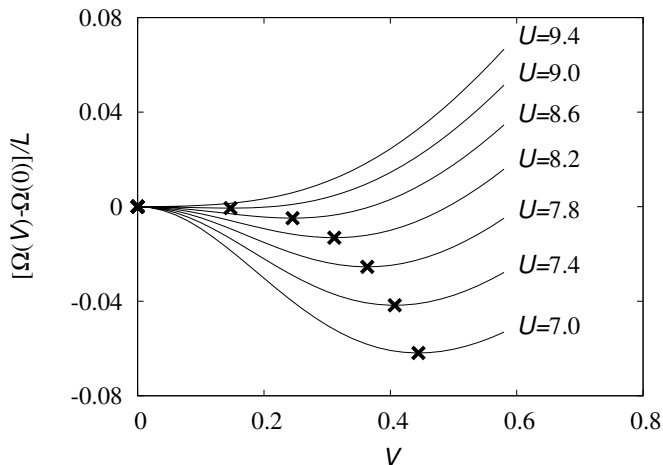


FIG. 1: The grand potential $\Omega(V)$ for the two-orbital model ($M = 2$) as a function of V for different U at $T = 0$. Crosses correspond to stationary points.

Fig. 1, we show the grand potential at zero temperature for several values of the Coulomb interaction U . When U is small, the grand potential has a minimum at finite V . Thus the effective bandwidth is finite, stabilizing the metallic ground state. It is seen that the stationary point moves towards the origin continuously with increasing U . For large U , the minimum is located at the origin, indicating that the Mott insulating state is stabilized by strong electron correlations. In the vicinity of the critical point U_c , the grand potential can be expanded in powers of V ,

$$\Omega(V) = \Omega(0) + AV^2 + \mathcal{O}(V^4). \quad (14)$$

Therefore, the critical point separating the metallic and the insulating phases is characterized by the condition $A = 0$.³⁴ By solving this analytically, we obtain the self-consistent equation for the critical point U_c as,

$$U_c = -\frac{100}{39} \int_{-\infty}^0 [z - \xi(z, U_c)] \rho(z) dz$$

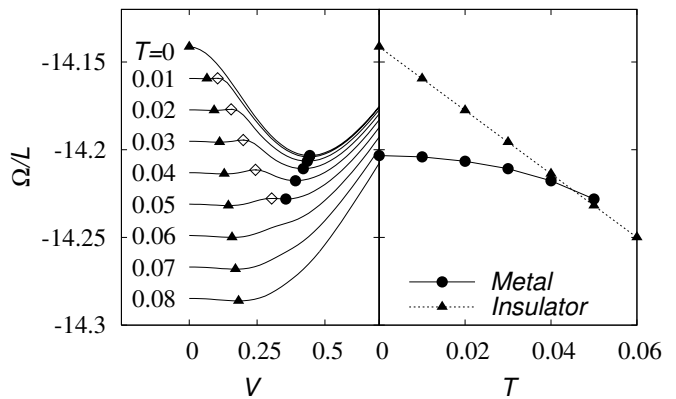


FIG. 2: (*left panel*) The grand potential Ω as a function of the effective hybridization V for $U = 7$. Closed circles and triangles represent the stationary points for the metallic and the Mott insulating states. Diamonds denote unstable stationary points. (*right panel*) Stationary values of the grand potential as a function of the temperature T for $U = 7$. Symbols are the same as in the left panel.

$$-\frac{U_c}{39} \int_{-\infty}^{\infty} \frac{317U_c + 83\xi(z, U_c)}{[17U_c + 8\xi(z, U_c)]\xi(z, U_c)} \rho(z) dz \quad (15)$$

with $\xi(z, U) = \sqrt{U^2 + z^2}$. The detail of the derivation is shown in Appendix A. The critical point $U_c \simeq 9.217$ thus obtained is more accurate than the results ($U_c = 10$) estimated by the two-site DMFT method.⁴¹

We now consider the competition between the metallic and the Mott insulating phases at finite temperatures, following the way for the single band case.³⁴ The grand potential is shown in Fig. 2 at finite temperatures. It is seen that two minima appear at low temperatures. One of the minima is located at larger V , which corresponds to the metallic solution, since it is continuously connected to the metallic one at zero temperature. The other is adiabatically connected to $V = 0$ at zero temperature, so that this solution characterizes the Mott insulating state. Such a double-well structure at low temperatures causes the first-order transition accompanied by hysteresis. In fact, as increasing temperature, the stationary point for the metallic state disappears around $T_{c2} = 0.05$, where the Mott transition occurs to the insulating phase. On the other hand, as decreasing temperature, the Mott insulating phase realized at high temperatures is stable except for zero temperature, since the corresponding local minimum always exists at finite temperatures. The first-order transition temperature $T_c = 0.045$ for $U = 7$ is determined by the crossing point of the two minima in the grand potential, as shown in Fig. 2. This hysteresis induced by the first-order transition is also observed when the interaction U is varied. We show the effective hybridization V at $T = 0.04$ in Fig. 3. Starting from the metallic state, the increase of the Coulomb interaction decreases the effective hybridization V , and finally triggers the Mott transition to the insulating phase at $U_{c2} = 7.2$, where we observe the discontinuity in V . On

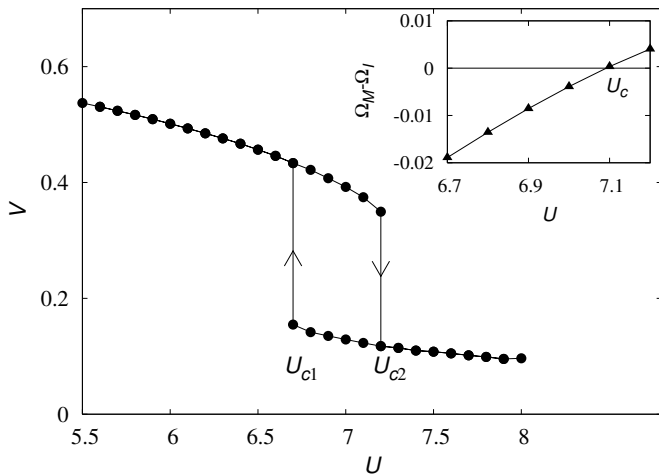


FIG. 3: The effective hybridization V as a function of U at $T = 0.04$. Inset shows the grand potential as a function of U at $T = 0.04$, where Ω_M (Ω_I) is the grand potential for the metallic (insulating) state.

the contrary, the Mott transition occurs at $U_{c1} = 6.7$ when the interaction decreases. In this parameter regime, the level crossing in the minima of the grand potential appears at $U_c = 7.1$ (inset of Fig. 3), which defines the first-order transition point at $T = 0.04$.

We have seen here that the two-orbital Hubbard model exhibits qualitatively similar properties to the single-band case^{5,34} as far as the nature of the Mott transitions is concerned. In the following section, we give more quantitative discussions about the Mott transitions by using the phase diagrams obtained for the multi-orbital Hubbard model with $M = 1 \sim 4$.

IV. PHASE DIAGRAMS OF MULTI-ORBITAL SYSTEMS

We now determine the phase diagrams of the multi-orbital Hubbard model. We first calculate the renormalization factor $Z = (1 - \partial\Sigma(\omega)/\partial\omega)^{-1}$, which is inversely proportional to the effective mass, to characterize the metallic ground state at zero temperature. The results are shown in Fig. 4. The introduction of the Coulomb interaction decreases the renormalization factor, making the mass of quasi-particles heavier. In the small U region, there is not a big difference in the behavior of Z among different M cases. If we look at Z in more detail (inset of Fig. 4), the mass gets slightly heavier (smaller Z) as M increases. This comes from the fact that the electron correlations are somewhat enhanced for multi-orbital cases by the inter-orbital Coulomb interaction. On the other hand, further increase of the Coulomb interaction leads to quite different behavior: as the number of orbitals M increases, the mass is less renormalized, which makes the metallic state more stable up to large U .^{42,43,44} This implies that the inter-orbital interaction enhances orbital

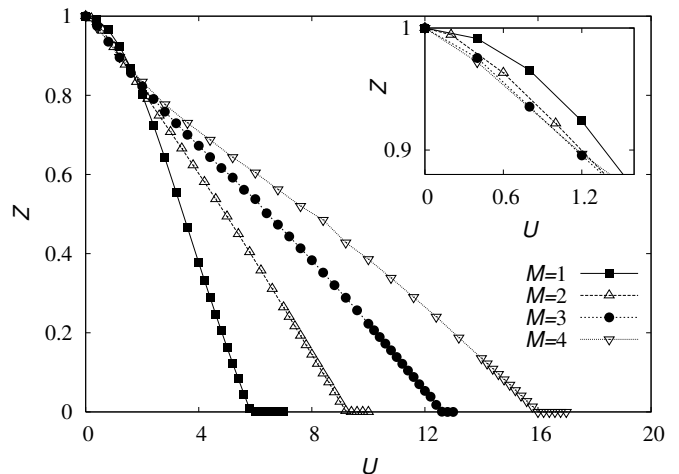


FIG. 4: The quasi-particle weight Z as a function of the Coulomb interaction U for the system with $M = 1, 2, 3, 4$ at $T = 0$. The inset is the enlarged figure in the small U region.

fluctuations for large U , which in turn stabilize the metallic state, as pointed out in the two-orbital case.⁴¹ In fact, the critical points $U_{c2}(T = 0) = 9.2173, 12.6044$ and 15.9958 for $M = 2, 3$ and 4 (see Appendix), are much larger than $U_c = 5.84$ for the single-orbital model.³⁴ Therefore, enhanced orbital fluctuations play a key role to stabilize the metallic state at zero temperature.

We now move to the finite-temperature properties. The phase diagrams obtained in the way mentioned in the previous section are shown in Fig. 5. There are three

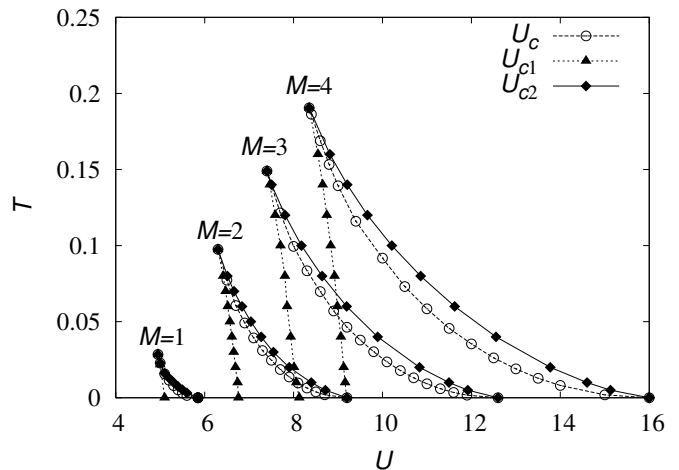


FIG. 5: Phase diagrams for the degenerate Hubbard model with the orbital degeneracy $M = 1, 2, 3, 4$.

phase boundaries for each system, U_{c1} , U_{c2} and U_c . The double-well structure in the grand potential gives rise to two kinds of transitions with the discontinuity in the physical quantities. On the phase boundary $U_{c1}(U_{c2})$, the Mott transition occurs from the insulating (metallic) state to the metallic (insulating) state as U decreases (increases). The area surrounded by U_{c1} and U_{c2} is re-

ferred to as the coexistence phase.^{5,34} The critical point U_c is determined so that the two minima of the grand potential take the same value. At zero temperature, the critical points U_c and U_{c2} merge to give the continuous Mott transition, because the double-well structure disappears at $T = 0$. Therefore, the introduction of the temperature drastically changes the phase boundary as discussed in the single-orbital case.^{5,34} It is found that as temperature increases, the phase boundaries U_{c1} , U_{c2} , and U_c merge at the critical temperature T_c , where the second-order phase transition occurs.

The above characteristic properties in the Mott transitions are qualitatively the same as the single-orbital case. We now discuss the effects due to orbital fluctuations quantitatively. First note that the coexistence region bounded by the phase boundaries U_{c1} and U_{c2} is enlarged when the number of orbital M increases. Furthermore, we see that the M -dependence of the critical points U_{c1} , $U_c(T_c)$ and the critical temperature T_c is different from that of U_{c2} . To clarify this point, the critical values are plotted as a function of M in Fig. 6. It is found that

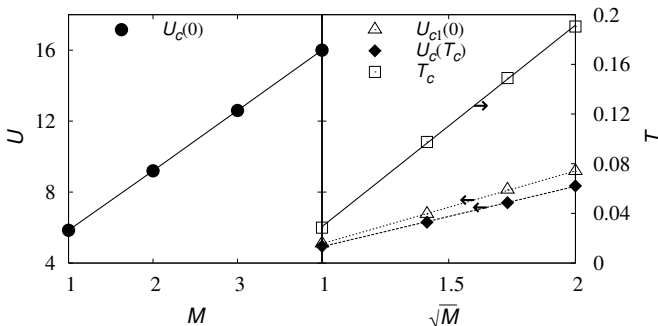


FIG. 6: The critical points $U_c(T = 0)$, $U_c(T = T_c)$, $U_{c1}(T \rightarrow 0)$ and the critical temperature T_c as a function of the orbital degeneracy M .

U_{c2} is proportional to the orbital degeneracy M , while U_{c1} and $U_c(T_c)$ the square root of M . These results are consistent with the previous results.^{23,31,42,43,44} However, we wish to note that the finite-temperature properties such as the phase diagrams have not been clarified quantitatively so far. In particular, the results on the M -dependence of the critical temperature T_c obtained here are beyond the qualitative discussions by Florens *et al.*,⁴⁴ who obtained only the upper bound for $T_c \propto M$.

To conclude this section, we would like to briefly discuss the effects of the Hund exchange coupling. For this purpose, we add the following term to the Hamiltonian (3),

$$\begin{aligned}
 \mathcal{H}_J = & -J \sum_i \sum_{\alpha < \alpha'} \sum_{\sigma} n_{i\alpha\sigma} n_{i\alpha'\sigma} \\
 & -J \sum_i \sum_{\alpha < \alpha'} (c_{i\alpha\uparrow}^\dagger c_{i\alpha\downarrow} c_{i\alpha'\downarrow}^\dagger c_{i\alpha'\uparrow} + H.c.) \\
 & -J \sum_i \sum_{\alpha < \alpha'} (c_{i\alpha\uparrow}^\dagger c_{i\alpha\downarrow}^\dagger c_{i\alpha'\uparrow} c_{i\alpha'\downarrow} + H.c.) \quad (16)
 \end{aligned}$$

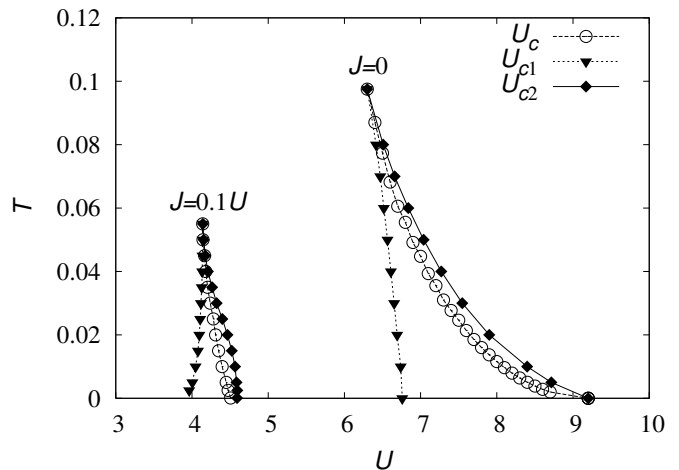


FIG. 7: Phase diagrams for the two-orbital Hubbard model with the Hund coupling $J = 0.1U$ under the condition $U = U' + 2J$. For clarity, we also show the results at $J = 0$.

with $J > 0$, where we impose the condition $U = U' + 2J$ due to the symmetry requirement. Since the calculation gets somewhat difficult in the presence of J , we show the results obtained for the representative case of $M = 2$. The obtained phase diagram is shown in Fig. 7 and compared with the $J = 0$ case. First, we notice that upon introducing J , the phase boundaries are immediately shifted to the weak-interaction regime, and therefore the metallic state gets unstable for large U . Correspondingly, the coexistence region surrounded by the first order transitions shrinks as J increases. This remarkable tendency indeed reflects the fact that the metallic state is stabilized by enhanced orbital fluctuations in the case of $U = U'$: the Hund coupling suppresses such orbital fluctuations, and stabilizes the Mott-insulating phase. Another point to be mentioned is that the Mott transition becomes of first-order even at zero temperature in the presence of J ,^{22,31,32} since the subtle balance realized at $T = 0$ in the case of $U = U'$ is not kept anymore for finite J . Since there is another claim that the second order transition is possible for certain choices of parameters at $T = 0$,³² which may depend on the strength of Hund coupling, we need further detailed discussions to clarify this problem. Although we have presented only the results for the $M = 2$ case, we expect that the effects of J on the phase diagram should be essentially the same as shown here: the introduction of J suppresses orbital fluctuations, thus favors the Mott insulating phase even in the small U regime. It also shrinks the coexistence phase dramatically.

V. SUMMARY

We have investigated the Mott transitions in the multi-orbital Hubbard model at zero and finite temperatures by means of the self-energy functional approach. By choos-

ing the Anderson impurity model as a reference system, we have discussed how the orbital degeneracy affects the nature of the Mott transitions. We have obtained the finite-temperature phase diagram for the system having $M(\leq 4)$ degenerate bands. Although the phase diagrams show qualitatively similar features irrespective of the orbital degeneracy, there are some remarkable effects due to degenerate orbitals. In particular, it has been shown that enhanced orbital fluctuations make the metallic phase more stable even at finite temperatures. Therefore, if such fluctuations are suppressed, the metallic state is expected to be unstable, which has been shown to be the case by considering the system with the Hund coupling. Also, it has quantitatively been clarified how distinctly the M -dependence appears in the critical points U_{c1} and U_{c2} : the critical point U_{c1} depends on the square root of the orbital degeneracy M , while the critical point U_{c2} is proportional to M . This analysis concludes that the critical temperature T_c is proportional to the square root of M , which may be important to understand the Mott transitions in the real materials with orbital degeneracy.

The self-energy functional approach used in the paper allows quantitatively reliable discussions for multi-orbital systems at finite temperatures. Since this formalism provides a tractable way to incorporate spin and charge ordered states, which have been neglected in this paper, it may be used for more detailed study of the finite-temperature properties in multi-orbital Mott systems.

Acknowledgments

Numerical computations were carried out at the Super-computer Center, the Institute for Solid State Physics, University of Tokyo. This work was supported by a Grant-in-Aid for Scientific Research from the Ministry of Education, Culture, Sports, Science, and Technology, Japan.

APPENDIX A

We analytically determine the critical value of U for the Mott transition in the multi-orbital Hubbard model at zero temperature. The grand potential Eq. (10) is rewritten as

$$\begin{aligned} \Omega/L = & \Omega_{\text{imp}} + 2M \sum_i \int dz \rho(z) \omega_i(z) \theta[-\omega_i(z)] \\ & - 2M \sum_i \omega_i \theta(-\omega'_i), \end{aligned} \quad (\text{A1})$$

where Ω_{imp} is the grand potential of the reference system and $\theta(x)$ is the step function. $\omega'_i, \omega_i(z)$ are the poles of the impurity Green's function of the reference system, $G'(\omega)$, and the approximated Green function of the original system, $G(\omega; z) = 1/(\omega + \mu - z - \Sigma(\omega))$, respectively.

First we consider the two-orbital system. In the atomic limit $V = 0$, the Green's function and the self-energy at the impurity site for the reference system are given by

$$G'_{\text{atom}}(\omega) = \frac{1}{2} \left[\frac{1}{\omega - U/2} + \frac{1}{\omega + U/2} \right] \quad (\text{A2})$$

$$\Sigma_{\text{atom}}(\omega) = \mu + \frac{U^2}{4\omega}, \quad (\text{A3})$$

where the poles of G'_{atom} are $\pm U/2$. Then the Green's function of the original lattice model is given by

$$G_{\text{atom}}^{-1}(\omega; z) = \omega - z + \frac{U^2}{4\omega}, \quad (\text{A4})$$

which has the poles at

$$\omega_{\pm}(z) = \frac{1}{2} \left(z \pm \sqrt{z^2 + U^2} \right). \quad (\text{A5})$$

As discussed in the text, we can expand the quantities in V around the atomic limit. The grand potential is $\Omega' = -2U - 24V^2/U + \mathcal{O}(V^4)$. We also analyze the Green's functions $G'(\omega)$ and $G(\omega; z)$ around the atomic limit and obtain their poles up to the second order in V . Here we need only the poles in the negative energy region, because the poles in the positive energy region do not affect Ω , see Eq. (A1). The Green's functions $G'(\omega)$ and $G(\omega; z)$ have eight poles in the $M = 2$ case, and thus four poles in the negative region. The negative poles of $G'(\omega)$ are

$$\begin{aligned} \omega'_1 &= -10 \frac{V^2}{U} + \mathcal{O}(V^4), \\ \omega'_2 &= -\frac{U}{2} - (30 + 4\sqrt{3}) \frac{V^2}{U} + \mathcal{O}(V^4), \\ \omega'_3 &= -\frac{U}{2} - (30 - 4\sqrt{3}) \frac{V^2}{U} + \mathcal{O}(V^4), \\ \omega'_4 &= -2U - 26 \frac{V^2}{U} + \mathcal{O}(V^4), \end{aligned}$$

and the negative poles of $G(\omega; z)$ are

$$\begin{aligned} \omega_1(z) &= 100zV^2/U^2 + \mathcal{O}(V^4), \\ \omega_2(z) &= \omega_-(z) + B(z/U) V^2/U + \mathcal{O}(V^4), \\ \omega_3(z) &= -U/2 - 30V^2/U + \mathcal{O}(V^4), \\ \omega_4(z) &= -2U - \frac{168z + 390U}{15U + 8z} V^2/U + \mathcal{O}(V^4), \end{aligned} \quad (\text{A6})$$

where

$$B(x) = -\frac{6525 + 8714x^2 - 3200x^4}{(225 - 64x^2)\sqrt{1 + x^2}} - \frac{50x(237 - 64x^2)}{225 - 64x^2}. \quad (\text{A7})$$

The grand potential is written down as

$$\Omega/L = -4 \int_{-\infty}^{\infty} dz \rho(z) \xi(z, U)$$

$$\begin{aligned}
& + \frac{4V^2}{U^2} \left\{ 39U + 100 \int_{-\infty}^0 dz \rho(z) (z - \xi(z, U)) \right. \\
& \left. + U \int_{-\infty}^{\infty} dz \rho(z) \frac{317U + 83\xi(z, U)}{[17U + 8\xi(z, U)]\xi(z, U)} \right\} + \mathcal{O}(V^4), \tag{A8}
\end{aligned}$$

where $\xi(z, U) = \sqrt{U^2 + z^2}$. The condition $\partial^2 \Omega / \partial V^2|_{V=0} = 0$ is satisfied at the Mott transition point U_c .³⁴ Given that the free density of state is symmetric $\rho(z) = \rho(-z)$, we derive the self-consistent equation for U_c , Eq. (15).

Similarly, we can analyze the cases of $M = 3$ and $M = 4$. The self-consistent equation for U_c at $M = 3$ reads

$$U_c = -\frac{49}{20} \int_{-\infty}^0 [z - \xi(z, U_c)] \rho(z) dz$$

$$-\frac{U_c}{80} \int_{-\infty}^{\infty} \frac{545U_c + 80\xi(z, U_c)}{[17U_c + 8\xi(z, U_c)]\xi(z, U_c)} \rho(z) dz, \tag{A9}$$

and at $M = 4$ is

$$\begin{aligned}
U_c &= -\frac{324}{135} \int_{-\infty}^0 [z - \xi(z, U_c)] \rho(z) dz \\
& - \frac{U_c}{135} \int_{-\infty}^{\infty} \frac{837U_c + 63\xi(z, U_c)}{[17U_c + 8\xi(z, U_c)]\xi(z, U_c)} \rho(z) dz. \tag{A10}
\end{aligned}$$

The solution of these equations gives the accurate values of the critical point: $U_c = 12.6044$ and 15.9958 for $M = 3$ and 4 , respectively.

-
- ¹ N. F. Mott, *Metal-Insulator Transition* (Taylor & Francis, London, 1990), 2nd ed.
- ² F. Gebhard, *The Mott Metal-Insulator Transition*, vol. 137 of *Springer Tracts in Modern Physics* (Springer, Berlin, 1997).
- ³ D. B. McWhan and A. Menth, Phys. Rev. Lett. **27**, 941 (1971); D. B. McWhan, A. Menth, J. P. Remeika, W. F. Brinkman and T. M. Rice, Phys. Rev. B **7**, 1920 (1973); S. A. Carter, T. F. Rosenbaum, J. M. Honig and J. Spalek, Phys. Rev. Lett. **67**, 3440 (1992); S. A. Carter, T. F. Rosenbaum, P. Metcalf, J. M. Honig and J. Spalek, Phys. Rev. B **48**, R16841 (1993).
- ⁴ M. Imada, A. Fujimori, and Y. Tokura, Rev. Mod. Phys. **70**, 1039 (1998).
- ⁵ A. Georges, G. Kotliar, W. Krauth, and M. J. Rozenberg, Rev. Mod. Phys. **68**, 13 (1996).
- ⁶ G. Kotliar and D. Vollhardt, Phys. Today **57**, 53 (2004).
- ⁷ Y. Tokura and N. Nagaosa, Science **288**, 462 (2000).
- ⁸ T. Katsufuji, Y. Taguchi, and Y. Tokura, Phys. Rev. B **56**, 10145 (1997).
- ⁹ M. Mochizuki and M. Imada, Phys. Rev. Lett. **91**, 167203 (2003).
- ¹⁰ V. I. Anisimov, I. A. Nekrasov, D. E. Kondakov, T. M. Rice, and M. Sigris, Eur. Phys. J. B **25**, 191 (2002).
- ¹¹ M. Sigris and M. Troyer, Eur. Phys. J. B **39**, 207 (2004).
- ¹² A. Liebsch, Phys. Rev. Lett. **91**, 226401 (2003); Europhys. Lett. **63**, 97 (2003); Phys. Rev. B **70**, 249904(E) (2004).
- ¹³ A. Koga, N. Kawakami, T.M. Rice and M. Sigris, Phys. Rev. Lett. **92**, 216402 (2004); cond-mat/0503651.
- ¹⁴ L. de' Medici, A. Georges, and S. Biermann, cond-mat/0503764.
- ¹⁵ R. Arita and K. Held, cond-mat/0504040.
- ¹⁶ M. Ferrero, F. Becca, M. Fabrizio, and M. Capone, cond-mat/0503759.
- ¹⁷ S. Nakatsuji *et al.*, Phys. Rev. Lett. **90**, 137202 (2003); S. Nakatsuji and Y. Maeno, Phys. Rev. Lett. **84**, 2666 (2000).
- ¹⁸ K. Sreedhar, *et al.*, J. Solid State Comm. **110** (1994) 208; Z. Zhang, *et al.*, J. Solid State Comm. **108**, 402 (1994); **117** (1995) 236.
- ¹⁹ Y. Kobayashi, S. Taniguchi, M. Kasai, M. Sato, T. Nishioaka, and M. Kontani, J. Phys. Soc. Jpn **65**, 3978 (1996).
- ²⁰ G. Kotliar and H. Kajueter, Phys. Rev. B **54**, R14221 (1996).
- ²¹ M. J. Rozenberg, Phys. Rev. B **55**, R4855 (1997).
- ²² J. Bünemann and W. Weber, Phys. Rev. B **55**, 4011 (1997); J. Bünemann and W. Weber and F. Gebhard, *ibid* **57**, 6896 (1998).
- ²³ H. Hasegawa, J. Phys. Soc. Jpn. **56**, 1196 (1997).
- ²⁴ K. Held and D. Vollhardt, Eur. Phys. J. B **5**, 473 (1998).
- ²⁵ J. E. Han, M. Jarrell, and D. L. Cox, Phys. Rev. B **58**, R4199 (1998).
- ²⁶ T. Momoi and K. Kubo, Phys. Rev. B **58**, R567 (1998).
- ²⁷ A. Klejnberg and J. Spalek, Phys. Rev. B **57**, 12041 (1998).
- ²⁸ Y. Imai and N. Kawakami, J. Phys. Soc. Jpn **70**, 2365 (2001).
- ²⁹ A. Koga and Y. Imai and N. Kawakami, Phys. Rev. B **66**, 165107 (2002); A. Koga *et al.*, J. Phys. Soc. Jpn. **72**, 1306 (2003).
- ³⁰ Y. Ono, R. Bulla and A. C. Hewson, Eur. Phys. J. B **19**, 375 (2001); Y. Ohashi and Y. Ono, J. Phys. Soc. Jpn. **70**, 2989 (2001).
- ³¹ Y. Ono, M. Potthoff, and R. Bulla, Phys. Rev. B **67**, 035119 (2003).
- ³² T. Pruschke and R. Bulla, cond-mat/0411186.
- ³³ M. Potthoff, Phys. Rev. B **64**, 165114 (2001).
- ³⁴ M. Potthoff, Eur. Phys. J. B **32**, 429 (2003); M. Potthoff, *ibid* **36**, 335 (2003); K. Pozgajčić, cond-mat/0407172.
- ³⁵ M. Potthoff, cond-mat/0406671; M. Potthoff, cond-mat/0503715.
- ³⁶ J. M. Luttinger, Phys. Rev. **118**, 1417 (1960).
- ³⁷ R. Bulla and M. Potthoff, Eur. Phys. J. B **13**, 257 (2000).
- ³⁸ M. Caffarel and W. Krauth, Phys. Rev. Lett. **72**, 1545 (1994).
- ³⁹ G. Moeller, Q. Si, G. Kotliar, M. Rozenberg, and D. S. Fisher, Phys. Rev. Lett. **74**, 2082 (1995).
- ⁴⁰ R. Bulla, Phys. Rev. Lett. **83**, 136 (1999).
- ⁴¹ A. Koga, Y. Imai, and N. Kawakami, Phys. Rev. B **66**, 165107 (2002).
- ⁴² J.P. Lu, Phys. Rev. B **49**, 5687 (1994).
- ⁴³ R. Frésard and G. Kotliar, Phys. Rev. B **56**, 12909 (1997); R. Frésard and M. Lamboley, J. Low. Temp. Phys. **126**, 1091 (2002).
- ⁴⁴ S. Florens, A. Georges, G. Kotliar, and O. Parcollet, Phys. Rev. B **66**, 205102 (2002).